Carbon 96 (2016) 1053–1059

Contents lists available at ScienceDirect

Carbon

journal homepage: www.elsevier.com/locate/carbon

Binder-free polymer encapsulated sulfur–carbon nanotube composite cathodes for high performance lithium batteries

Weibang Kong [a], Li Sun [a], Yang Wu [a], Kaili Jiang [a, b], Qunqing Li [a, b], Jiaping Wang [a, b, *], Shoushan Fan [a]

[a] Department of Physics and Tsinghua-Foxconn Nanotechnology Research Center, Tsinghua University, Beijing 100084, China
[b] Collaborative Innovation Center of Quantum Matter, Beijing 100084, China

ARTICLE INFO

Article history:
Received 7 September 2015
Received in revised form
14 October 2015
Accepted 18 October 2015
Available online 21 October 2015

ABSTRACT

Binder-free polymer encapsulated nano sulfur/super-aligned CNT (PVP@S-SACNT) composite electrode is developed via a solution-based method. In the composite structure, PVP not only facilitates better dispersion of SACNT bundles into a 3D continuous network, but also encapsulates the sulfur nanoparticles onto the SACNT network to ensure their tight electrical connection and prevent polysulfide dissolution. Combining the advantages of the high conductive and porous SACNT network and the PVP surface modification, the PVP@S-SACNT cathode exhibits excellent cyclic stability (initial capacity of 1303 mA h g^{-1} and 856 mA h g^{-1} after 200 cycles at 1 C) and high-rate performance (590 mA h g^{-1} at 20 C). Moreover, the PVP@S-SACNT composite presents excellent long-term capacity stability with a capacity decay of 0.052% per cycle during 1000 charge/discharge cycles at 2 C. With these appealing performances, the PVP@S-SACNT composite becomes a promising cathode material for the next-generation rechargeable batteries.

1. Introduction

With the rapid development of portable electronics and electrical vehicles, it is urgently needed to develop rechargeable batteries with high energy density for next generation energy-storage system [1,2]. As one of the promising candidates, sulfur cathode in lithium–sulfur (Li–S) batteries exhibits superior theoretical specific capacity (1672 mA h g^{-1}) and high energy density (2600 W h kg^{-1}) based on the electrochemical reaction of $S_8 + 16Li^+ + 16e^- \rightarrow 8Li_2S$, which are much larger than those of conventional lithium ion batteries based on metal oxide cathodes such as $LiCoO_2$ [3]. In addition, sulfur cathode demonstrates several advantages of natural abundance, low cost, safe operating voltage (~2.15 V), and non-toxicity. However, the commercialization of Li–S batteries is restricted by several problems, including the poor electrical conductivity of both sulfur and Li_2S, the large volume expansion of sulfur (~80%) during its lithiation, and the dissolution of the intermediate lithium polysulfides (Li_2S_n, $4 \leq n \leq 8$) into the electrolyte [4,5]. These problems lead to low coulombic efficiency and poor cyclic performance of Li–S batteries.

In order to address these challenges, various methods have been developed in purpose of improving the conductivity of sulfur electrode, ensuring well distribution of sulfur in the electrode, and preventing the dissolution of polysulfides [6–9]. One general approach is to confine sulfur within conductive carbon materials [10–16], such as porous carbon, graphene, carbon nanotube (CNT), etc. Among these carbon materials, CNTs have drawn much attention due to its 1D flexible nanostructure, which is suitable for the construction of continuous porous structure and flexible CNT-S composite electrode [17–21]. Compared to other approaches to prepare binder-free cathode for Li–S batteries, such as the three-dimensional sulfur/graphene multifunctional hybrid sponges [14], coaxial graphene wrapping over sulfur-coated carbon nanofibers [15], sandwich-structured sulfur cathode [22], binder-free cathode based on CNTs allows a simplified synthesis procedure due to highly entangled structures formed by 1D tubes and more homogeneous distribution of sulfur that benefits both electron and ion transfer in the electrode. Various binder/current collector free electrodes based on CNTs were reported [18–20], including the S-CNT film [18], the self-weaving S-MWCNT composite [19], and the vertical aligned CNT/S composite [20], etc. Though impressive

* Corresponding author. Department of Physics and Tsinghua-Foxconn Nanotechnology Research Center, Tsinghua University, Beijing 100084, China.
E-mail address: jpwang@tsinghua.edu.cn (J. Wang).

http://dx.doi.org/10.1016/j.carbon.2015.10.062
0008-6223/

capacities within 100 charge–discharge cycles were revealed in these CNT based sulfur cathodes, long-term cycle stability and high rate performance should be improved. To increase the high-rate performance of sulfur cathodes, nano S-SACNT composite electrode was prepared by our group by anchoring sulfur nanoparticles on the network of super-aligned CNTs (SACNTs) via a solution-based method [21]. Compared with ordinary CNTs, SACNTs exhibit distinguished properties in terms of its "super-aligned" nature, large aspect ratio (~10^4), clean surface, and the ability to form a robust and continuous network due to the strong van der Waals force among tubes and bundles [23–26]. These characteristics of SACNTs contributes to a 3D conductive network with excellent mechanical strength and flexibility, which not only provided continuous transporting paths for electrons and lithium ions but also served as an ideal container for accommodating and trapping the polysulfides. High initial capacity, cyclic stability, and high rate performance were demonstrated in nano S-SACNT composite structures. However, polysulfides can still dissolve into the electrolyte through the relatively open structures of CNTs during long-term cycling, leading to capacity fade in prolonged cycles.

Apart from the modification of sulfur cathodes by carbon materials, polymer additives or functional groups have also been introduced to sulfur cathodes to improve the electrochemical kinetics as well as further encapsulate the polysulfides [10,13,27–30]. For example, Zhang's group introduced a polyethylene (PEG) barrier into aligned S-CNT electrode and obtained electrochemical performances superior to the pristine cathode without PEG layer [27]. Zhang's group modified sulfur–graphene oxide cathode with cetyltrimethyl ammonium bromide (CTAB) that attained a long life of 1500 cycles with a low decay rate [33]. Cui's group utilized polyvinylpyrrolidone (PVP) as template and surface modification agent to obtain carbon–sulfur composite cathodes with greatly enhanced cycling performance [6,32]. As a supplement to carbon materials, polymer additives provide additional physical/chemical confinement to block the diffusion of polysulfides, leading to improved cyclic stability [13,27,30–36]. However, in order to provide sufficient physical barrier to polysulfides, large amount of polymer additives is usually involved in these electrodes, which might decrease the electrical conductivity of the sulfur cathode and deteriorate its capacity and rate performance.

In this work, by combining the advantages of conductive SACNT network and polymer additives, binder-free PVP-encapsulated S-SACNT composite cathode (PVP@S-SACNT) was designed in purpose of providing both high conductivity and efficient confinement for sulfur/polysulfides and thus leading to excellent cyclic stability and high-rate performance. The PVP@S-SACNT composite was constructed by in-situ anchoring sulfur nanoparticles onto the SACNT network via a simple solution-based reaction in presence of PVP. PVP is an amphiphilic polymer with a hydrophobic alkyl backbone and hydrophilic amide groups that can be used as a dispersing agent. PVP not only facilitated better dispersion of SACNT bundles into a 3D continuous network with excellent electrical and mechanical properties, but also encapsulated the sulfur nanoparticles onto the SACNT network to ensure their tight electrical connection and prevent polysulfide dissolution. The PVP@S-SACNT composite cathode presented excellent cyclic stability (initial capacity of 1303 mA h g^{-1} and 856 mA h g^{-1} after 200 cycles at 1 C, a capacity decay of 0.052% per cycle during 1000 charge/discharge cycles at 2 C) and high-rate performance (590 mA h g^{-1} at 20 C).

2. Experimental

2.1. Fabrication of SACNT arrays

SACNT arrays with a tube diameter of 20–30 nm and a height of 300 μm were synthesized on silicon wafers by chemical vapor deposition with iron as the catalyst and acetylene as precursor. Details of the synthesis procedure can be found in previous papers [23–25].

2.2. Fabrication of the PVP@S-SACNT, S-SACNT, and PVP@S-CNT composite electrodes

30 mg SACNTs and 222.2 mg sodium thiosulfate (Alfa Aesar) were dispersed in 60 mL deionized water with PVP (Alfa Aesar) at concentrations of 0.2 wt%, 0.5 wt%, and 1 wt% by intensive ultrasonication (1000 W) for 60 min. Then, 60 mL hydrochloric acid with a concentration of 3 M was slowly added under strong magnetic stirring at 70 °C for 0.5 h to allow for the sulfur precipitation onto SACNTs. After washing with deionized water and drying at 50 °C, binder-free PVP@S-SACNT electrode was obtained. For comparison, S-SACNT composite electrode was prepared without adding PVP. Ordinary CNTs were used to fabricate the PVP@S-CNT composite following the same procedure as the PVP@S-SACNT electrode. Then, the powders were mixed with PVDF binder at a weight ratio of 90:10 in the N-methyl-2-pyrrolidine solution, and the slurry was coated on an aluminum foil to form the PVP@S-CNT electrode.

2.3. Morphology and structure characterization

The crystalline structure of the PVP@S-SACNT composite was characterized by XRD using a diffractometer (Rigaku, Cu Kα radiation). TGA tests were conducted using a Pyris 1 TGA (Perkin Elmer, USA) at a heating rate of 10 °C min^{-1} between 25 and 500 °C in air. The structure and composition of the PVP@S-SACNT, S-SACNT, and PVP@S-CNT composites were characterized by SEM (Sirion 200, FEI) and TEM (Tecnai G2F20, FEI). Tensile tests of the PVP@S-SACNT and S-SACNT composites were performed using an Instron 5848 microtester with a strain rate of 1% per min and a 1 cm gauge length.

2.4. Electrochemical test

Coin-type (CR 2016) half-cells with these composites as the working electrode and pure lithium foil as the reference electrode, were assembled in a glove box filled with protective argon gas (M. Braun inert gas systems Co. Ltd., Germany). A polypropylene film (Celgard 2400) was used as separator. 1 M LiTFSI solution in dioxolane (DOL) and dimethoxyethane (DME) mixed at a volume ratio of 1:1 with addition of 0.2 M $LiNO_3$ was used as electrolyte. The cyclic voltammetry tests and electrochemical impedance spectroscopy (EIS) measurements were performed using a Potentiostat/Galvanostat instrument (Princeton PARStat 2273). The charge/discharge measurements were carried on the Land battery test system (Wuhan Land Electronic Co., China) within the voltage window of 1.8–2.6 V at different charge/discharge rates at room temperature. The PVP@S-SACNT electrode after cycling test was washed with the mixed DOL and DME solution for several times and dried for further microstructure characterization.

3. Results and discussion

The PVP@S-SACNT composite was fabricated via a simple solution-based method. Fig. 1 schematically illustrates the synthesis procedure. SACNT arrays expanded into a well-dispersed 3D network by ultrasonication in the aqueous sodium thiosulfate solution in presence of PVP. Then hydrochloric acid was dropped into the SACNT-PVP-sodium thiosulfate mixture. Based on a simple reaction between sodium thiosulfate and hydrochloric acid ($Na_2S_2O_3 + 2HCl \rightarrow S + SO_2 + 2NaCl + H_2O$), sulfur nanoparticles

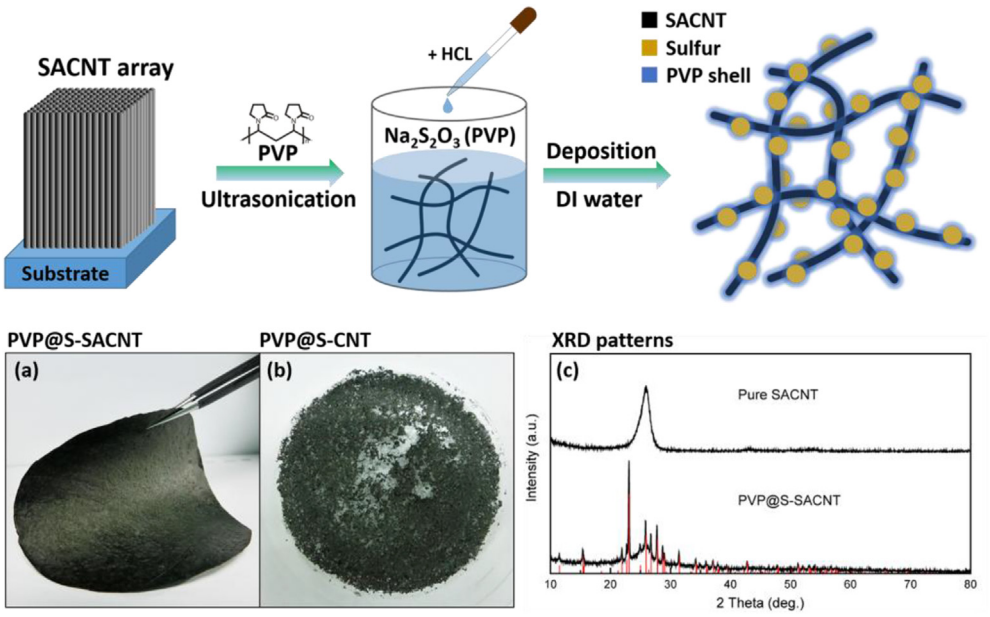

Fig. 1. Schematic of the synthesis procedure for the PVP@S-SACNT composite. Photographs of (a) the PVP@S-SACNT and (b) the PVP@S-CNT composites; (c) XRD patterns of pure SACNT and the PVP@S-SACNT composite. (A color version of this figure can be viewed online).

uniformly anchored onto the SACNT network, and a thin PVP shell encapsulated both SACNTs and sulfur nanoparticles. After washing with deionized water and drying, a freestanding, binder-free, and flexible PVP@S-SACNT cathode was obtained (Fig. 1a). Note that SACNTs with high purity and strong van der Waals force among tubes and the formation of a continuous network are very important in obtaining the binder-free electrode. Following the same procedures, ordinary CNTs with random orientation could not interweave to a network, and the PVP@S-CNT composite collapsed into powders (Fig. 1b) instead of forming a continuous film. Severe aggregation of CNTs and bulk sulfur particles with sizes up to 5 μm were observed in the PVP@S-CNT composite as shown in Supplementary data (Fig. S1). S-SACNT composite without PVP modification (S-SACNT) was also fabricated for comparison. All these composites had almost the same sulfur content.

The X-ray diffraction (XRD) analysis was conducted on pure SACNTs and the PVP@S-SACNT composite. As shown in Fig. 1c, the characteristic (002) peak at 26° of CNT was observed in both pure SACNTs and the PVP@S-SACNT composite. The other diffraction peaks were in good accordance with those of *Fddd* orthorhombic sulfur (S8, PDF#08-0247) as plotted by the red column lines, illustrating the crystallized feature of the sulfur nanoparticles. As PVP was added to a very small amount, peaks of PVP were not observed in the XRD pattern. Thermogravimetric analysis (TGA) analysis of the PVP@S-SACNT composite showed weight losses of 47% at 250 °C and 4% at 350 °C (Fig. S2), corresponding to the evaporation of sulfur and PVP, respectively. Therefore, the contents of sulfur and PVP were determined to be approximately 47 wt% and 4 wt% in the PVP@S-SACNT composite. The active sulfur loading of the electrode was about 1.0 mg cm^{-2}.

Fig. 2a showed the typical scanning electron microscopy (SEM) image of the top surface of the S-SACNT composite electrode. Without PVP modification, bundles of SACNTs were formed, which gave rise to large pore size, rough surface, and aggregation of sulfur as marked by arrows. Transmission electron microscopy (TEM) image in Fig. 2b revealed that the sulfur particles were mostly with a diameter of ~150 nm. Compared with the S-SACNT composite, the PVP@S-SACNT composite presented superior structure characteristics as shown in Fig. 2c, d, e, and f. Fig. 2c and its inset demonstrated a smooth and sub-micro porous structure without aggregation of sulfur or bundling of SACNTs. This porous SACNT network was expected to accommodate the volume change of sulfur and avoid the aggregation of S/Li_2S during the cycling. Furthermore, the interweaved and homogeneous microstructures of the PVP@S-SACNT composites also lead to a robust structure with improved mechanical property. As illustrated by the stress–strain curves of the PVP@S-SACNT and S-SACNT composites in Fig. S3, a strength of 13.61 MPa and a Young's modulus of 135.15 MPa were obtained in the PVP@S-SACNT composite. In comparison, the S-SACNT composite exhibited a much smaller strength of 1.45 MPa and a Young's modulus of 26.68 MPa. Besides, the strain of the PVP@S-SACNT composite at the maximum strength was 15.0%, higher than that of the S-SACNT (13.3%), indicating the improved flexibility of the PVP@S-SACNT composite. The distinguished mechanical properties of the PVP@S-SACNT composites benefit from the mutual effect of the SACNT interweaved network and PVP modification (Fig. 2c).

The energy-dispersive X-ray spectroscopy (EDS) mapping (Fig. 2d) demonstrated that elemental C, S, N, and O were uniformly dispersed across the SACNT network, suggesting a uniform distribution of sulfur, PVP, and SACNTs in the composite. The TEM image of the PVP@S-SACNT composite (Fig. 2e) showed that sulfur nanoparticles were homogeneously embedded in the SACNT network. The diameters of the sulfur nanoparticles were mostly 10–25 nm, which was much smaller than that in the S-SACNT composite (~150 nm). The smaller grain size of sulfur in the PVP@S-SACNT composite could be attributed to the PVP surface modification. Due to the amphiphilic feature, PVP not only acted as dispersant to allow homogeneous dispersion of SACNTs in the sodium thiosulfate solution, but also served as a protective template to avoid aggregation and growth of sulfur particles. The high magnification TEM image of the PVP@S-SACNT composite (Fig. 2f) and the EDS mapping (Fig. S4) indicated that both SACNT and sulfur particle were uniformly coated by a 2 nm thick PVP layer. With the PVP encapsulation, sulfur nanoparticles anchored tightly onto the SACNT network, thus benefiting the efficient electron transfer and

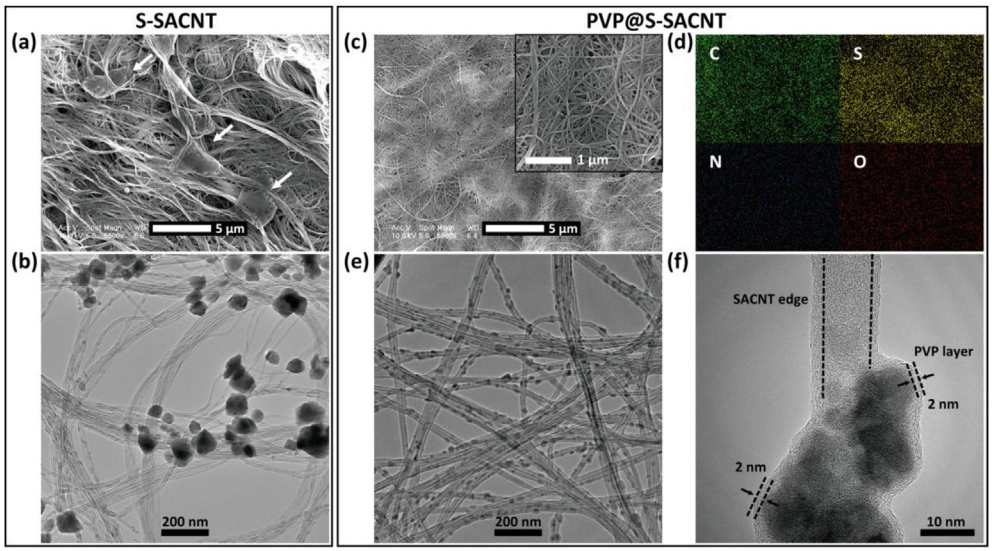

Fig. 2. (a) SEM and (b) TEM images of the S-SACNT composite, showing aggregation of sulfur and SACNTs; (c) SEM image and (d) EDS mapping of the PVP@S-SACNT composite, showing its smooth and porous morphology and homogeneous dispersion of S, SACNT, PVP; (e) TEM and (f) high magnification TEM images of the PVP@S-SACNT composite, demonstrating the uniform anchoring of sulfur nanoparticles on SACNTs and a thin PVP layer coated on both sulfur nanoparticle and SACNT. (A color version of this figure can be viewed online).

increasing the electrochemical kinetics. Moreover, PVP formed a protective layer around SACNTs and sulfur, which can effectively suppress the diffusion of polysulfides during the cathode reaction. Previous research suggested that the oxygenated groups in PVP exhibited high binding strength with Li_xS compounds during the cycling reaction [32], which might prevent the aggregation of Li_2S_2 and Li_2S.

The cyclic voltammetry (CV) profiles of the PVP@S-SACNT and S-SACNT composites are shown in Fig. 3. For the PVP@S-SACNT composite, two reduction peaks at approximately 2.30 V and 2.05 V were observed, corresponding to the reaction from S_8 to Li_2S_4 and from Li_2S_4 to Li_2S_2/Li_2S, respectively (Fig. 3a). After the initial activation in the first cycle, the position and magnitude of the redox peaks remained almost unchanged for 100 cycles, demonstrating the high electrochemical kinetics and excellent cyclic stability of the PVP@S-SACNT composite. With the PVP shell covering the surfaces of both sulfur particles and SACNT network, the polysulfides could be well confined and the aggregation of Li_2S/S could be effectively avoided during cycling, as illustrated in Fig. 3a inset. In contrast, as schematically shown in Fig. 3b inset, without the protection from the PVP layer, sulfur particles had weak connection with the SACNT network, and suffered from severe side-reaction with the electrolyte, polysulfides dissolution, and sulfur loss, as indicated by the broad reduction peaks from 1.80 V to 2.10 V and the shoulder of the oxidation peak at 2.35 V in the CV profile (Fig. 3b).

The cyclic performance of the PVP@S-SACNT, S-SACNT, and PVP@S-CNT composites were tested at 1 C. Before cycling at 1 C, the batteries were first cycled at 0.5 C for 5 cycles to activate the electrochemical reaction. As shown in Fig. 4a, the PVP@S-SACNT composite exhibited a large initial capacity of 1303 mA h g^{-1} at 0.5 C. When the charge/discharge rates were changed to 1 C, a capacity of 1175 mA h g^{-1} was obtained with capacity retention of 856 mA h g^{-1} after 200 cycles. The morphology of the PVP@S-SACNT composite electrode had almost no change after 100 cycles at 1 C (Fig. S5), demonstrating the outstanding mechanical property and cyclic stability of the composite. In contrast, the S-SACNT composite without PVP modification showed fast capacity decay from 921 mA h g^{-1} to 441 mA h g^{-1} after 200 cycles due to the severe shuttle effect and the aggregation of S/Li_2S during the charge/discharge processes. The PVP@S-CNT composite showed the worst performance, with a capacity of only 393 mA h g^{-1} after 200 cycles, due to its inhomogeneous microstructure and severe sulfur aggregation. The excellent cycling performances of the PVP@S-SACNT composite could be ascribed to the three key roles of PVP. Firstly, as a dispersing agent, PVP ensured a sufficient dispersion of

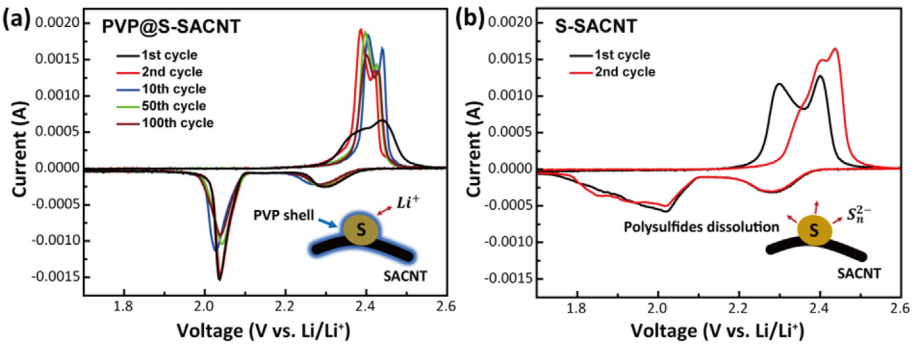

Fig. 3. CV profiles of the (a) PVP@S-SACNT and (b) S-SACNT composites. (A color version of this figure can be viewed online).

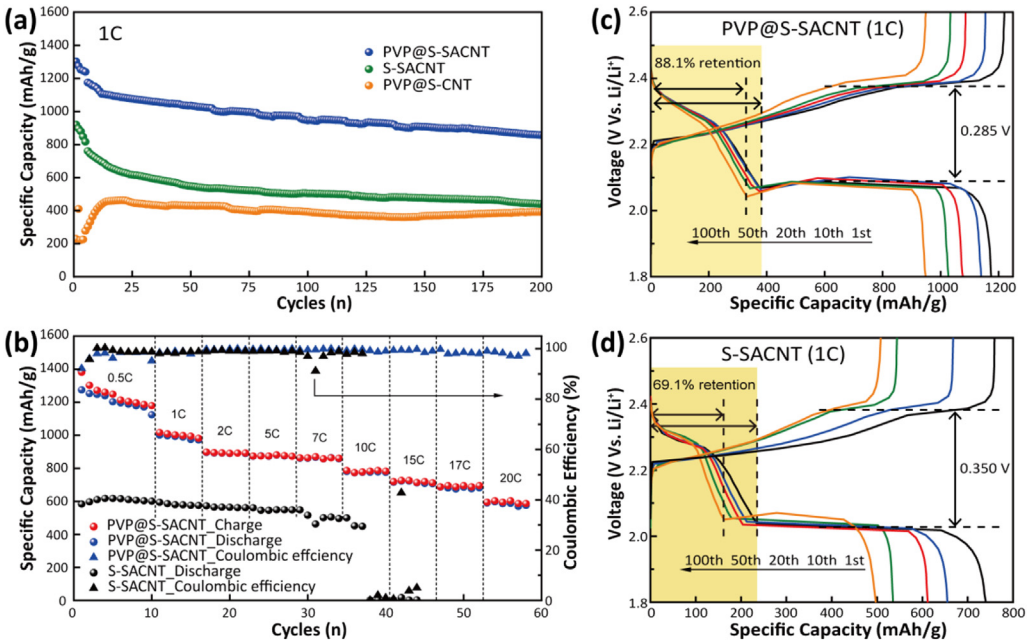

Fig. 4. (a) Cyclic performance of the PVP@S-SACNT, S-SACNT, and PVP@S-CNT composites at charge/discharge rate of 1 C. (b) Rate performance of the PVP@S-SACNT and the S-SACNT composites. Charge and discharge voltage profiles of the (c) PVP@S-SACNT and (d) S-SACNT composites at 1st, 10th, 20th, 50th, and 100th cycles. (A color version of this figure can be viewed online).

the nonpolar SACNTs by modifying the surface of SACNTs. Secondly, the PVP molecules in the aqueous solution assembled with each other through hydrophobic interaction to form a protect template [37], which allowed the sulfur nanoparticles to adhere tightly onto the SACNTs, as well as avoided the sulfur aggregation. Thirdly, the PVP molecules could physically encapsulate the nano S-SACNT composite, and chemically improve the polysulfide-trapping capability by restraining the lithium polysulfides to the carbon surface, as suggested in literature [32]. Moreover, based on the robust SACNT network, the binder-free PVP@S-SACNT composite showed high conductivity and excellent mechanical properties, which are beneficial for cycling stability.

It should be mentioned that the cycling behavior of the PVP@S-SACNT composites is highly related to the concentration of PVP in the synthesis process that affected the morphologies of the composites, as shown in Fig. S6. The aforementioned PVP@S-SACNT composite was prepared with a PVP concentration of 0.5 wt%, showing uniform anchoring of sulfur nanoparticles onto the SACNT network (Fig. 2c, e, and Fig. S6b). When PVP was added to a smaller concentration of 0.2 wt%, SACNTs were not sufficiently dispersed and sulfur particles were not well constrained by the SACNT network and the PVP template. Therefore, bundles of SACNTs and aggregation of sulfur could still be observed on the surface (marked by arrows in Fig. S6a), resulting in its low capacity of 763 mA h g^{-1} after 200 cycles at 1 C, which is inferior to that with a PVP concentration of 0.5 wt% (856 mA h g^{-1}), as shown in Fig. S6d. When PVP was added to a high concentration of 1 wt%, the excess PVP may self-aggregate and result in growth of micrometer sized sulfur particles on the SACNT network (marked by arrows in Fig. S6c). Besides, the large amount of PVP with low electronic conductivity also limited the electron transfer behavior and gave rise to its low capacity with fast decay (463 mA h g^{-1} after 200 cycles at 1 C). Both of the composites had the same sulfur content as the PVP@S-SACNT composite with 0.5 wt% PVP concentration. These results suggested that the concentration of PVP significantly affected the performance of the PVP@S-SACNT composite electrodes and it was optimized to be 0.5 wt% in this study.

Owing to the high conductivity of the well-dispersed SACNT network and the surface modification of sulfur nanoparticles by PVP, the PVP@S-SACNT composite cathode exhibited excellent rate performance. As shown in Fig. 4b, at a constant discharge rate of 0.5 C, the PVP@S-SACNT composite presented high reversible discharge capacities of 1275, 1001, 896, 873, 781, and 590 mA h g^{-1} at the stepwise charge rates of 0.5 C, 1 C, 2 C, 5 C, 10 C, and 20 C, respectively. Moreover, even at 20 C, the PVP@S-SACNT composite cathode showed an extremely high coulombic efficiency of nearly 100%. The voltage profiles of the PVP@S-SACNT composite at different rates were showed in Fig. S7. As the charge current increased at the stepwise rates from 0.5 C to 20 C, the polarized charge voltage plateau increased. Even if the charge rate increased to 20 C, the cell could still be charged to nearly 600 mA h g^{-1}, which demonstrated the excellent electrochemical properties. As a contrast, the discharge capacities of the S-SACNT composite without PVP modification at different charge rates started from about 600 mA h g^{-1} at 0.5 C and collapsed at 10 C. The voltage/testing time profiles were showed in Fig. S8. The S-SACNT composite without PVP modification could not afford 10 C charge rate, then collapsed.

Fig. 4c shows the charge/discharge profiles of the PVP@S-SACNT composite cathode for up to 100 cycles at 1 C, exhibiting two discharge plateaus. The upper discharge plateau at 2.30 V represented the fast reduction from S_8 to long-chain polysulfides (Li_2S_x, $4 < x < 8$), and the lower discharge plateau at 2.05 V corresponded to the conversion from polysulfides to Li_2S_2/Li_2S. Generally, the decay of capacity contribution from the upper discharge plateau indicates the extent of polysulfides dissolution. The overlapped upper discharge plateaus from the initial cycle to the 100th cycle revealed that the PVP encapsulation acted a key role to confine the polysulfides diffusion. The capacity retention of the upper plateau of the PVP@S-SACNT composite was 88.1% after 100 cycles at 1 C (Fig. 4c), compared to only 69.1% for the S-SACNT composite without PVP modification (Fig. 4d), showing an outstanding

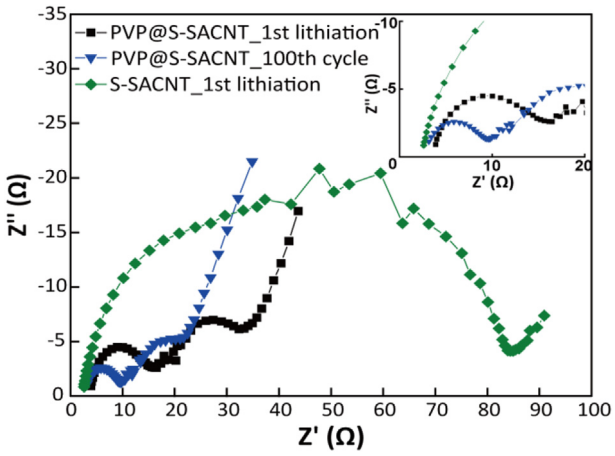

Fig. 5. EIS spectra of the PVP@S-SACNT and the S-SACNT composites. (A color version of this figure can be viewed online).

polysulfide-trapping capability of PVP. The lower discharge plateau of the PVP@S-SACNT composite at 2.05 V was stable and flat, indicating the high reaction kinetic and capacity contribution of approximately 800 mA h g^{-1} from this plateau (Fig. 4c). There existed a discharge activation process where the lower discharge plateau started. Due to the insolubility and low Li-ion diffusivity of Li_2S_2 and Li_2S, this discharge progress needs an activated energy for the nucleation, which required high electron/ion conductivity of the cathode materials and tight connection between S/Li_2S and the conductive agent [4,5]. As shown in Fig. 4c, little change was found in the position of these activation points after 100 cycles, revealing that the PVP encapsulation provided a tight electrical connection between sulfur nanoparticles and SACNT network and ensured efficient electron and ion transfer. The PVP encapsulation also continuously trapped the polysulfides diffusion and provided high electrochemical reversibility and kinetics for the flat and stable discharge plateau. Moreover, the PVP@S-SACNT composite showed less voltage hysteresis of 0.285 V than the S-SACNT composite (0.350 V), which were ascribed to the PVP modified nanostructure of the composite.

Electrochemical impedance spectroscopy (EIS) was conducted to the PVP@S-SACNT and S-SACNT composites. The semicircles at the high frequency range in Fig. 5 demonstrated that the PVP@S-SACNT composite had a much smaller charge transfer resistance (~15 Ω) compared with the S-SACNT composite (~85 Ω) after the first lithiation. Comparing with the S-SACNT composite, the small charge transfer resistance of the PVP@S-SACNT composite was attributed to the nanosize of sulfur particles and their tight connection with SACNTs by the PVP encapsulation (Fig. 2e, f). The charge transfer resistance decreased to approximately 7 Ω after 100 cycles at 1 C rate, which proved that the porous structure of the PVP@S-SACNT composite provided efficient paths for the insertion/extraction of the Li-ion and the PVP modification continuously improved the electrochemical performance of the Li–S cell. On the other hand, the PVP modification slightly increased the ohmic resistance of the cell, which might be caused by the low conductivity of PVP. The ohmic resistance also decreased after cycling, illustrating that the electrolyte well infiltrated into the porous structure of the PVP@S-SACNT composite after the activation process for the initial cycles as shown in CV profile (Fig. 3a). The depressed semicircles at lower frequency range might be attributed to the formation of the small amount of the insoluble polysulfides species, which dominated the lower voltage plateau [6,38,39].

The PVP@S-SACNT composite also exhibited excellent long-term cyclic stability. As shown in Fig. 6, discharge capacities of around 464 and 311 mA h g^{-1} could be obtained after 1000 cycles at charge/discharge rates of 1 C and 2 C, respectively, corresponding to the capacity decay of as low as 0.054% and 0.052% per cycle. Meanwhile, the cells also maintained a high coulombic efficiency of almost 100% during the long-term cycling test.

The PVP@S-SACNT composite has several advantages as a novel cathode for lithium sulfur batteries: (1) The amphiphilic feature of the PVP molecules ensures the formation of a smooth and porous structure of the SACNT network, thus promoting the efficient transfer of both electrons and Li-ions and avoiding the aggregation of the Li_2S/S during cycling. (2) The PVP molecules serve as a protective template for the uniform anchoring of the sulfur nanoparticles onto the SACNT network, resulting in high electrochemical kinetics. (3) The PVP surface encapsulation physically and chemically modifies the nano S-SACNT composite and continuously traps the polysulfides during the charge/discharge cycling. (4) Without additional conductive agent and current collector, the robust SACNT network facilitates the facile synthesis of binder-free, highly conductive, and flexible electrodes, thus dramatically increasing the specific energy.

4. Conclusion

In summary, we develop a binder-free PVP encapsulated nano S-SACNT composite electrode via a solution-based method. Taking the advantages of the high conductive and porous SACNT network and the PVP surface modification, the PVP@S-SACNT composite exhibits excellent cyclic stability, with an initial discharge capacity of 1303 mA h g^{-1} and a capacity of 856 mA h g^{-1} after 200 cycles at 1 C. Favorable high-rate performance is also revealed, with a capacity as high as 590 mA h g^{-1} at the charge rate of 20 C. Moreover, the PVP@S-SACNT composite presents excellent long-term stability

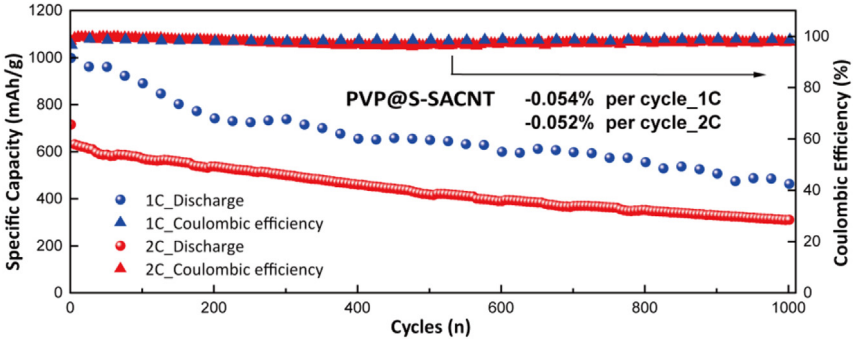

Fig. 6. Long term cyclic performance of the PVP@S-SACNT composite at charge/discharge rates of 1 C and 2 C. (A color version of this figure can be viewed online).

with a capacity decay of 0.052% per cycle during 1000 charge/discharge cycles at 2 C. Ascribed to the superior microstructure characteristic and the PVP surface encapsulation, the PVP@S-SACNT composite also exhibits outstanding electrochemical kinetics, along with high coulombic efficiencies of almost 100% in both long-cycling and high-rate testing. Besides, the simple fabrication technique and the freestanding and flexible properties make the PVP@S-SACNT composite electrode of great potential for large-scale production. With these appealing performances, the PVP@S-SACNT composite becomes a promising cathode material for the next-generation rechargeable batteries.

Acknowledgments

This work was supported by the National Basic Research Program of China (2012CB932301), NSFC (51102146 and 51472141), and the NCET Program of China.

Appendix A. Supplementary data

Supplementary data related to this article can be found at http://dx.doi.org/10.1016/j.carbon.2015.10.062.

References

[1] M. Armand, J.M. Tarascon, Building better batteries, Nature 451 (2008) 652–657.
[2] B. Dunn, H. Kamath, J.M. Tarascon, Electrical energy storage for the grid: a battery of choices, Science 334 (2011) 928–935.
[3] X.L. Ji, L.F. Nazar, Advances in Li–S batteries, J. Mater. Chem. 20 (2010) 9821–9826.
[4] A. Manthiram, Y.Z. Fu, S.H. Chung, C. Zu, Y.S. Su, Rechargeable lithium-sulfur batteries, Chem. Rev. 114 (2014) 11751–11787.
[5] Y.X. Yin, S. Xin, Y.G. Guo, L.J. Wan, Lithium-sulfur batteries: electrochemistry, materials, and prospects, Angew. Chem. Int. Ed. 52 (2013) 13186–13200.
[6] W.Y. Li, G.Y. Zheng, Y. Yang, Z.W. Seh, N. Liu, Y. Cui, High-performance hollow sulfur nanostructured battery cathode through a scalable, room temperature, one-step, bottom-up approach, PNAS 110 (2013) 7148–7153.
[7] W.D. Zhou, Y.C. Yu, H. Chen, F.J. DiSalvo, H.D. Abruña, Yolk-shell structure of polyaniline-coated sulfur for lithium-sulfur batteries, J. Am. Chem. Soc. 135 (2013) 16736–16743.
[8] W.Y. Li, Q.F. Zhang, G.Y. Zheng, Z.W. Seh, H.B. Yao, Y. Cui, Understanding the role of different conductive polymers in improving the nanostructured sulfur cathode performance, Nano Lett. 13 (2013) 5534–5540.
[9] Z.W. Seh, W. Li, J.J. Cha, G. Zheng, Y. Yang, M.T. McDowell, et al., Sulphur-TiO2 yolk–shell nanoarchitecture with internal void space for long-cycle lithium-sulphur batteries, Nat. Commun. 4 (2013) 1331–1336.
[10] X. Ji, K.T. Lee, L.F. Nazar, A highly ordered nanostructured carbon-sulphur cathode for lithium-sulphur batteries, Nat. Mater. 8 (2009) 500–506.
[11] L.W. Ji, M.M. Rao, S. Aloni, L. Wang, E.J. Cairns, Y.G. Zhang, Porous carbon nanofiber-sulfur composite electrodes for lithium/sulfur cells, Energy Environ. Sci. 4 (2011) 5053–5059.
[12] H.J. Peng, J.Q. Huang, M.Q. Zhao, Q. Zhang, X.B. Cheng, X.Y. Liu, et al., Nanoarchitectured graphene/CNT@porous carbon with extraordinary electrical conductivity and interconnected micro/mesopores for lithium-sulfur batteries, Adv. Funct. Mater. 24 (2014) 2772–2781.
[13] H.L. Wang, Y. Yang, Y.Y. Liang, J.T. Robinson, Y.G. Li, A. Jackson, et al., Graphene-wrapped sulfur particles as a rechargeable lithium-sulfur battery cathode material with high capacity and cycling stability, Nano Lett. 11 (2011) 2644–2647.
[14] S. Lu, Y. Chen, X. Wu, Z. Wang, Y. Li, Three-dimensional sulfur/graphene multifunctional hybrid sponges for lithium-sulfur batteries with large areal mass loading, Sci. Rep. 4 (2014) 4629–4632.
[15] S. Lu, Y. Cheng, X. Wu, J. Liu, Significantly improved long-cycle stability in high-rate Li–S batteries enabled by coaxial graphene wrapping over sulfur-coated carbon nanofibers, Nano Lett. 13 (2013) 2485–2489.
[16] Y.C. Qiu, W.F. Li, W. Zhao, G.Z. Li, Y. Hou, M.N. Liu, et al., High-rate, ultralong cycle-life lithium/sulfur batteries enabled by nitrogen-doped graphene, Nano Lett. 14 (2014) 4821–4827.
[17] C. Tang, Q. Zhang, M.Q. Zhao, J.Q. Huang, X.B. Cheng, G.L. Tian, et al., Nitrogen-doped aligned carbon nanotube/graphene sandwiches: facile catalytic growth on bifunctional natural catalysts and their applications as scaffolds for high-rate lithium-sulfur batteries, Adv. Mater. 26 (2014) 6100–6105.
[18] K.K. Jin, X.F. Zhou, L.Z. Zhang, X. Xin, G.H. Wang, Z.P. Liu, Sulfur/carbon nanotube composite film as a flexible cathode for lithium-sulfur batteries, J. Phys. Chem. C 117 (2013) 21112–21119.
[19] Y.S. Su, Y. Fu, A. Manthiram, Self-weaving sulfur–carbon composite cathodes for high rate lithium-sulfur batteries, Phys. Chem. Chem. Phys. 14 (2012) 14495–14499.
[20] S. Dorfler, M. Hagen, H. Althues, J. Tubke, K. Kaskel, M.J. Hoffmann, High capacity vertical aligned carbon nanotube/sulfur composite cathodes for lithium-sulfur batteries, Chem. Commun. 48 (2012) 4097–4099.
[21] L. Sun, M.Y. Li, Y. Jiang, W.B. Kong, K.L. Jiang, J.P. Wang, et al., Sulfur nanocrystals confined in carbon nanotube network as a binder-free electrode for high-performance lithium sulfur batteries, Nano Lett. 14 (2014) 4044–4049.
[22] J. Song, Z. Yu, T. Xu, S. Chen, H. Sohn, M. Regula, et al., Flexible freestanding sandwich-structured sulfur cathode with superior performance for lithium-sulfur batteries, J. Mater. Chem. A 2 (2014) 8623–8627.
[23] K.L. Jiang, Q.Q. Li, S.S. Fan, Nanotechnology: spinning continuous carbon nanotube yarns, Nature 419 (2002) 801.
[24] K. Liu, Y.H. Sun, L. Chen, C. Feng, X.F. Feng, K.L. Jiang, et al., Controlled growth of super-aligned carbon nanotube arrays for spinning continuous unidirectional sheets with tunable physical properties, Nano Lett. 8 (2008) 700–705.
[25] K. Liu, K.L. Jiang, Y. Wei, S.P. Ge, P. Liu, S.S. Fan, Controlled termination of the growth of vertically aligned carbon nanotube arrays, Adv. Mater. 19 (2007) 975–978.
[26] S. Luo, K. Wang, J.P. Wang, K.L. Jiang, Q.Q. Li, S.S. Fan, Binder-free $LiCoO_2$/carbon nanotube cathodes for high-performance lithium ion batteries, Adv. Mater. 24 (2012) 2294–2298.
[27] J.Q. Huang, Q. Zhang, S.M. Zhang, X.F. Liu, W. Zhu, W.Z. Qian, et al., Aligned sulfur-coated carbon nanotubes with a polyethylene glycol barrier at one end for use as a high efficiency sulfur cathode, Carbon 58 (2013) 99–106.
[28] J. Song, T. Xu, M.L. Gordin, P. Zhu, D. Lv, Y.B. Jiang, et al., Nitrogen-doped mesoporous carbon promoted chemical adsorption of sulfur and fabrication of high-areal-capacity sulfur cathode with exceptional cycling stability for lithium-sulfur batteries, Adv. Funct. Mater. 24 (2014) 1243–1250.
[29] L.W. Ji, M.M. Rao, H.M. Zheng, L. Zhang, Y.C. Li, W.H. Duan, et al., Graphene oxide as a sulfur immobilizer in high performance lithium/sulfur cells, J. Am. Chem. Soc. 133 (2011) 18522–18525.
[30] S.M. Zhang, Q. Zhang, J.Q. Huang, X.F. Liu, W. Zhu, M.Q. Zhao, et al., Composite cathodes containing SWCNT@S coaxial nanocables: facile synthesis, surface modification, and enhanced performance for li-ion storage, Part. Part. Syst. Charact. 30 (2013) 158–165.
[31] S.H. Chung, A. Manthiram, A polyethylene glycol-supported microporous carbon coating as a polysulfide trap for utilizing pure sulfur cathodes in lithium-sulfur batteries, Adv. Mater. 26 (2014) 7352–7357.
[32] G.Y. Zheng, Q.F. Zhang, J.J. Cha, Y. Yang, W.Y. Li, Z.W. Seh, et al., Amphiphilic surface modification of hollow carbon nanofibers for improved cycle life of lithium sulfur batteries, Nano Lett. 13 (2013) 1265–1270.
[33] M.K. Song, Y.G. Zhang, E.J. Cairns, A long-life, high-rate lithium/sulfur cell: a multifaceted approach to enhancing cell performance, Nano Lett. 13 (2013) 5891–5899.
[34] M. Wang, W. Wang, A. Wang, K. Yuan, L. Miao, X. Zhang, et al., A multi-core–shell structured composite cathode material with a conductive polymer network for Li–S batteries, Chem. Commun. 49 (2013) 10263–10265.
[35] G.C. Li, G.R. Li, S.H. Ye, X.P. Gao, A polyaniline-coated sulfur/carbon composite with an enhanced high-rate capability as a cathode material for lithium/sulfur batteries, Adv. Energy Mater. 2 (2012) 1238–1245.
[36] F. Wu, J. Chen, L. Li, T. Zhao, R. Chen, Improvement of rate and cycle performance by rapid polyaniline coating of a MWCNT/sulfur cathode, J. Phys. Chem. C 115 (2011) 24411–24417.
[37] P.H. Qiu, C.B. Mao, Biomimetic branched hollow fibers templated by self-assembled fibrous polyvinylpyrrolidone structures in aqueous solution, ACS Nano 4 (2010) 1573–1579.
[38] C. Barchasz, J.C. Lepretre, F. Alloin, S. Patoux, New insights into the limiting parameters of the Li/S rechargeable cell, J. Power Sources 199 (2012) 322–330.
[39] L. Yuan, X. Qiu, L. Chen, W.J. Zhu, New insight into the discharge process of sulfur cathode by electrochemical impedance spectroscopy, J. Power Sources 189 (2009) 127–132.